

Integrative analysis reveals disrupted pathways regulated by microRNAs in cancer

Gary Wilk¹ and Rosemary Braun^{2,3,*}

¹Department of Chemical and Biological Engineering, Northwestern University, Evanston, IL 60208, USA

²Biostatistics Division, Feinberg School of Medicine, Northwestern University, Chicago, IL 60611, USA

³Department of Engineering Sciences and Applied Mathematics, Northwestern University, Evanston, IL 60208, USA

*To whom correspondence should be addressed. Tel: +312-503-3644; Email: rbraun@northwestern.edu

July 24, 2018

Abstract

MicroRNAs (miRNAs) are small endogenous regulatory molecules that modulate gene expression post-transcriptionally. Although differential expression of miRNAs have been implicated in many diseases (including cancers), the underlying mechanisms of action remain unclear. Because each miRNA can target multiple genes, miRNAs may potentially have functional implications for the overall behavior of entire pathways. Here we investigate the functional consequences of miRNA dysregulation through an integrative analysis of miRNA and mRNA expression data using a novel approach that incorporates pathway information *a priori*. By searching for miRNA–pathway associations that differ between healthy and tumor tissue, we identify specific relationships at the systems–level which are disrupted in cancer. Our approach is motivated by the hypothesis that if a miRNA and pathway are associated, then the expression of the miRNA and the collective behavior of the genes in a pathway will be correlated. As such, we first obtain an expression–based summary of pathway activity using Isomap, a dimension reduction method which can articulate nonlinear structure in high-dimensional data. We then search for miRNAs that exhibit differential correlations with the pathway summary between phenotypes as a means of finding aberrant miRNA–pathway coregulation in tumors. We apply our method to cancer data using gene and miRNA expression datasets from The Cancer Genome Atlas (TCGA) and compare $\sim 10^5$ miRNA–pathway relationships between healthy and tumor samples from four tissues (breast, prostate, lung, and liver). Many of the flagged pairs we identify have a biological basis for disruption in cancer.

1 Introduction

Cellular functions are carried out by coordinated regulation of genes on a pathway, which facilitate a series of interactions among genes to produce behaviors as diverse as cell metabolism to cell signaling. At the post-transcriptional level, microRNAs (miRNAs, miRs) modulate gene expression by binding to a 6-8 nucleotide target motif of mRNA transcripts, preventing translation and/or inducing degradation of their target genes. Due to the short binding motif, miRNA targeting is non-specific, such that a single miRNA may target multiple genes, and likewise, a single gene may be targeted by multiple miRNAs [1]. Currently, it is estimated

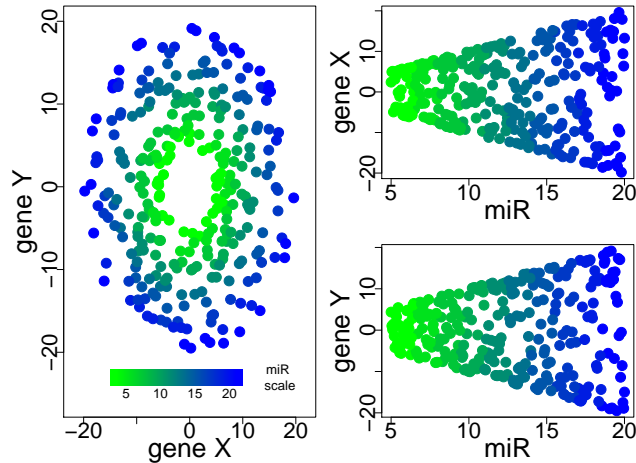


Figure 1: An example of two genes cycling out of phase with one-another, with the amplitude of the oscillation governed by the expression of a miRNA. The relationship is apparent in the left panel, where the lower values of the miRNA result in a smaller radius in the relationship between gene X and gene Y, yet neither gene X nor gene Y are correlated with the miRNA (right panels, top and bottom).

that $\sim 10^3$ known miRNAs regulate approximately a third of genes in the genome [2, 3, 4]. However, not all miRNA–gene relationships are known; studies to predict miRNA targets using sequence matching have had mixed success [5], and the functional consequences of miRNA dysregulation remains an area of active research. It is now thought that the multiplicity of targets enables miRNAs to exert a cumulative effect at the systems level, by targeting several genes and influencing their downstream interactions. miRNAs have been hypothesized to modulate pathways by regulating targets constituting those pathways [6, 7, 8, 9, 10]. Such systems–level control may explain the association of aberrant miRNA regulation with multiple diseases, including cancer [11, 12], endometriosis [13], inflammation [14], and several others.

High–throughput transcriptomics datasets now enable us to investigate the role of miRNAs in regulating pathway activity by integratively analyzing miRNA and gene expression from the same samples. Such analyses must address the challenges inherent to high–throughput data, including the fact that the number of features typically exceeds the number of samples by orders of magnitude, the data are inherently noisy, and many features may be irrelevant to the phenotype of interest. In addition, integrative analyses should account for the multiplicity of interactions that collectively contribute to phenotypic differences. Approaches for integrative miRNA–mRNA analysis generally fall into two categories [15]: (i) inferring interacting miR–mRNA pairs from transcriptomic data (e.g., by searching for high correlations [16], using regularized linear regression [17, 18], or mutual information [19]); and (ii) combining miRNA and mRNA expression data to identify a signature in the combined feature space that predicts the phenotype of interest [20, 21] (e.g., using non-negative matrix factorization [22] or clustering [23] to find combinations of miRNAs and genes that most strongly predict outcomes). A comprehensive review of integrative miRNA–mRNA analysis may be found in [15].

Information about gene interaction networks obtained from pathway databases (such as KEGG [24] or PID [25]) can be used to reduce dimensionality and improve interpretability by focusing on functionally

related gene sets. To date, however, most miRNA–mRNA integrative analyses do not explicitly incorporate this information *a priori*; instead, the interactions and signatures identified in the analysis are tested for overlap with known pathways at the end to lend a systems–level interpretation of the gene–level findings [26, 27]. Because many pathway analysis approaches (including enrichment methods such as GSEA [28]) rely on aggregating single–gene statistics rather than treating the pathway as a whole, they may miss crucial multi–gene interactions, such as the loss of coordinated expression. For example, the relevance of a miRNA that governs the relationship between two genes (such as the amplitude of the oscillation shown in Fig. 1) can be missed when considering the target genes in isolation, since neither gene is independently associated with the miRNA.

To overcome this limitation, several groups have proposed schemes to summarize gene expression across the pathway to quantify the overall level of pathway ‘activity’ in each sample [29, 30]. These approaches apply dimension reduction techniques (such as Singular Value Decomposition [SVD] and Principal Components Analysis [PCA]) to pre–defined gene sets, effectively yielding a single value that encapsulates the coarse coexpression behavior of all the genes in the pathway. In the PLAGe method [29], SVD was used to obtain a “pathway activity level” quantification based on the expression of genes in the pathway. A similar approach using PCA was employed in the GPC–Score [30] method. A nonlinear dimension reduction strategy for pathway summarization was considered in [31], which was shown to more faithfully summarize complex coexpression patterns than linear methods. More recently, the COMPADRE package [32] presented a framework for pathway summarization using a variety of dimension reduction techniques (including SVD, PCA, ICA, non–negative matrix factorization, and non–linear Isomap). The resulting pathway–level quantifications may then be tested for statistical associations with the phenotype, allowing the pathway to be treated as a single functional unit.

Here we propose a method that identifies miRNAs that differentially regulate the overall activity of pathways by using a pathway summarization technique capable of articulating nonlinear and multi–gene effects. Motivated by the observation that nonlinear dimension reduction can yield more accurate results when applied to gene expression data [33, 34, 31], our method uses Isomap [35], a nonlinear dimension reduction (NLDR) method, to summarize pathway expression to yield a low–dimensional summary that we call the Pathway Activity Summary (PAS). The PAS provides a faithful “snapshot” of the pathway, a coarse measure of pathway expression in all samples. Our method then computes correlation coefficients between PAS and miRNA expression to identify miRNAs whose expression is associated with the overall activity of the pathway. By comparing class–conditional correlations in cases and controls, we identify miRNA–pathway pairs that appear to have a differential relationship in cases and controls, elucidating the function of the miRNA and its potential mechanistic role in the phenotype of interest.

The approach used here is similar in some respects to our GPC–score method [30], which reveals novel regulatory relationships between genes and pathways. Using PCA for pathway summarization, GPC–score was able to identify differentially regulated gene–pathway pairs and accurately detect the interaction of genes with pathways that were not previously known to include them. The present work augments this prior analysis method in two novel ways. First, by using the nonlinear Isomap instead of PCA, we obtain a more faithful summary of pathway activity. Second, by applying the method to miRNA and mRNA data (rather than simply mRNA data), we achieve an integrative analysis of these datasets that can provide insight into the function of miRNAs. We apply this method to miRNA and mRNA expression profiles from four cancers (breast, liver, lung, and prostate) using data from The Cancer Genome Atlas (TCGA) [36].

Previous analyses have integrated multiple omics platforms to identify specific mechanisms regulating gene expression. Several pipelines have taken into account sample–specific data from TCGA at the transcriptomic, genomic, and epigenetic levels and have linked them with cell–generic data from other consortiums [37, 38]. These studies have identified relationships between expression regulators and genes in some cancer types. Recently, the TCGA Network surveyed miRNAs in the context of expression patterns and clinical outcomes in ovarian cancer, and found widespread impact on gene expression and molecular

heterogeneity [39]. Our method is also integrative, but novel in that it surveys miRNA regulation in the context of gene expression from a pathway perspective. Importantly, because our approach uses both miRNA and mRNA expression data, it avoids some of the pitfalls that were previously identified [40] with making pathway-level inferences from miRNA data alone.

In this study, we apply our methodology to gene and miRNA expression datasets from The Cancer Genome Atlas (TCGA) (<http://cancergenome.nih.gov/>), a freely accessible repository of high dimensional genomic and expression data for several cancers. The datasets include both tumor and adjacent-normal tissue samples across multiple experimental modalities. After identifying class-conditional correlation differences for all possible miRNA–pathway pairs, we assess their significance through permutation testing. We report miRNAs that appear to have pathway-wide effects whose relationships change with the development of cancer, and report results for multiple distinct cancers.

2 Materials and Methods

In order to elucidate the functional role of miRNAs in cancer, we seek to identify miRNAs that appear to influence the overall activity of a pathway, and whose effects on that pathway appear to differ between healthy and tumor tissue. To do so, we first compute a pathway activity summary for each sample in each pathway of interest using gene expression data. We then compute, class-conditionally, the correlation between the pathway expression summary and each miRNA in cases and controls to quantify the miRNA–pathway relationship in those tissues, and test whether tumor–normal differences in the miRNA–pathway correlations are statistically significant. We detail the steps of this algorithm below; a summary may be found in Table 1 and Figure 2.

2.1 Algorithm

To identify miRNAs whose effects across entire systems differ between two conditions, we compute the association of miRNAs with pathways and compare associations between phenotypes by correlating miRNA and pathway gene expression. Because a given pathway may comprise tens to hundreds of genes, we use Isomap [35] to compute a one-dimensional summary of gene expression across the pathway, which we call the Pathway Activity Summary (PAS). Here, each sample can be thought of as a point in a high-dimensional space whose coordinates correspond to the expression of the genes on that pathway. Because the underlying biology places constraints on the expression of these genes with respect to one another, we make the assumption that the samples lie on a low-dimensional manifold within the gene expression space. Isomap attempts to learn this manifold, yielding a coordinate that articulates the variability amongst samples; projecting the gene expression data from sample j onto this coordinate obtains the pathway activity score PAS_j for sample j across the pathway of interest. (The approach is analogous to that of PCA; in contrast to PCA, however, the Isomap coordinate need not be a linear transformation of the gene expression space.) By obtaining PAS values for each sample, we can then compare pathway activity in cases and controls, and test the association of pathway activity with other variables of interest.

Relationships between miRNA expression and pathway activity are then compared between phenotypes as follows. The correlation between the PAS for a pathway and expression for a miRNA is computed class-conditionally, i.e. separately for tumor and normal samples. We then compute the absolute difference of the miRNA–pathway correlation in tumor and normal tissue:

$$\Delta\rho(\text{miR}, \text{PAS}) = |\rho(\text{miR}, \text{PAS}|T) - \rho(\text{miR}, \text{PAS}|N)| \quad (1)$$

where $\rho(x, y)$ is the Spearman rank correlation between x and y , chosen for its insensitivity to outliers, and T and N indicate tumor and normal tissue, respectively. A large correlation difference $\Delta\rho$ between sample

Table 1: Procedure for assessing disrupted pathways regulated by miRNAs.

miRNA–pathway Algorithm

1. Subset gene expression data to the pathway genes, forming pathway expression matrix of l genes \times N samples.
2. Apply Isomap to pathway matrix using all samples, obtaining for each sample a PAS value based on the first Isomap coordinate (analogous to using the first principal component from PCA).
3. Compute the Spearman rank correlation between the miRNA and the PAS in tumor samples, $\rho(\text{miR}, \text{PAS}|T)$.
4. Compute the Spearman rank correlation between the miRNA and the PAS in normal samples, $\rho(\text{miR}, \text{PAS}|N)$.
5. Compute absolute correlation difference between phenotypes as shown in Equation 1.
6. Repeat steps 3-5 using randomly permuted phenotype labels for 10^5 resamplings to compute the null distribution of $\Delta\rho$'s.
7. Compare the true miRNA–pathway $\Delta\rho$ to the permuted null distribution obtained in step 6 to assess statistical significance of $\Delta\rho$.

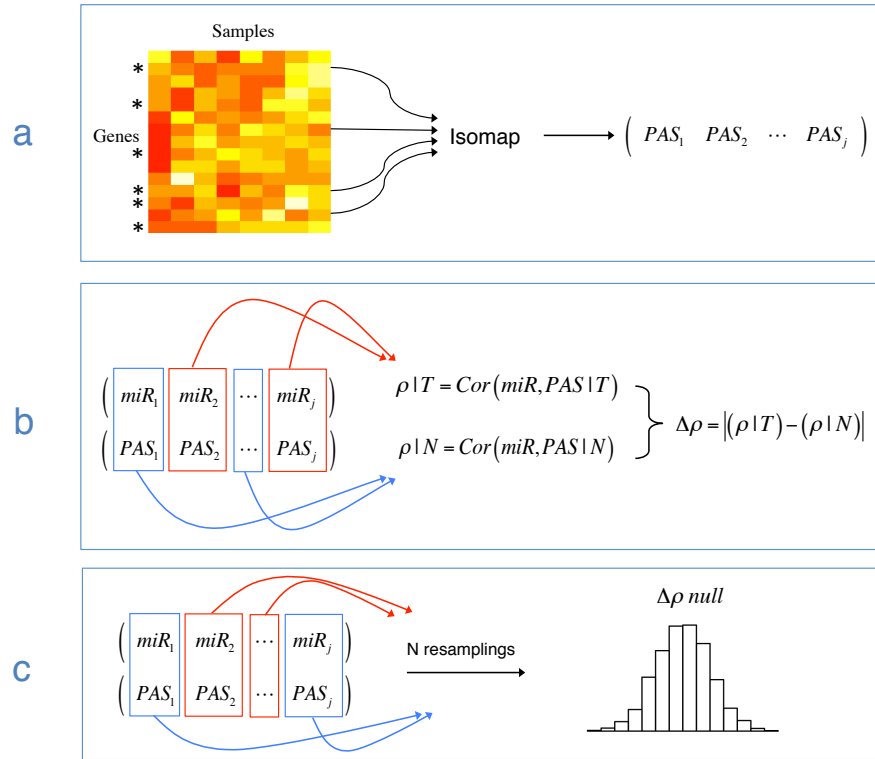


Figure 2: Illustration of the algorithm for a particular miRNA–pathway pair. (a) Gene expression data is first subsetted by the genes in a pathway and summarized by Isomap to produce the PAS, a one-dimensional summary of pathway expression in all samples. (b) PAS and miRNA expression are subsetted by phenotype, and miRNA–pathway correlations are computed for tumor and normal tissue. The difference between correlations gives $\Delta\rho$. (c) To assess $\Delta\rho$ significance, the $\Delta\rho$ null distribution is estimated by random permutation of the class labels.

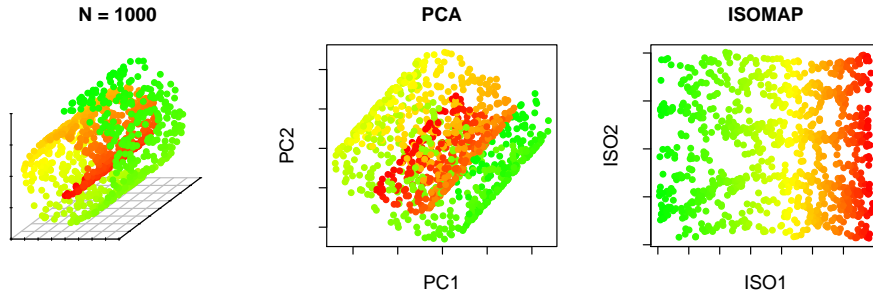


Figure 3: Swiss roll dimension reduction using PCA and Isomap. The roll is colored from green to red along the roll axis.

classes indicates apparent differential regulation of a pathway by a miRNA. Significance of the correlation difference is assessed by a permutation test, wherein the tumor and normal labels are randomly reassigned and Eq. 1 is recomputed to obtain a reference distribution for the miRNA–pathway pair. The steps for the algorithm are listed in Table 1. Figure 2 illustrates the algorithm in visual form.

2.2 Implementation

Here we detail the implementation of the algorithm as applied to mRNA and miRNA data from TCGA. Additional details are provided in the Supplementary Information.

2.2.1 Pathway summarization

The goal of pathway summarization is to reduce the dimensionality from that of l genes on the pathway to a single value that encapsulates the pathway activity for each sample. To this end, we define the PAS as the one-dimensional embedding of the pathway mRNA data using Isomap.

The choice to use Isomap for pathway summarization rather than SVD [29] or PCA [30] is motivated by its ability to articulate non-linear geometries in the data. A toy example comparing Isomap to PCA is shown in Figure 3. Here, the data lie on a two dimensional manifold that is coiled upon itself in 3-d space; dimension reduction via Isomap articulates this surface, whereas PCA cannot.

For each pathway in the KEGG [24] database, mRNA expression data are subsetted to the genes associated with that pathway to produce pathway-specific matrices. A total of 223 pathways are included in the analysis (after excluding six pathways with fewer than five genes). Expression levels for each gene are scaled to have zero mean and unit variance, allowing features to be measured on the same scale and reducing the disproportionate influence of any outlying samples. Isomap is then applied to the pathway gene expression data, and the projection of the sample on the first Isomap coordinate is used as a measure of the overall activity of the pathway.

An example of the utility of Isomap for summarizing gene expression data is given in Figure 4, where the 39-gene “Type I diabetes mellitus pathway” is summarized by PCA (left) and Isomap (right) for the TCGA breast cancer and normal tissue samples. Because Type I diabetes mellitus has been associated with an increased risk of breast cancer [41, 42] and several genes in the pathway are known tumor suppressors and cytokines that are commonly perturbed in tumors, we expect that a low dimensional embedding of the data should enable separation of the tumor and normal samples. However, we observe that this difference is not articulated using PCA; in the left scatterplot matrix of Figure 4, the red and black points overlap. By contrast, the Isomap embedding enables separation of the tumor and normal samples, suggesting that there exists a (nonlinear) pattern of gene expression within the pathway that is associated with breast cancer.

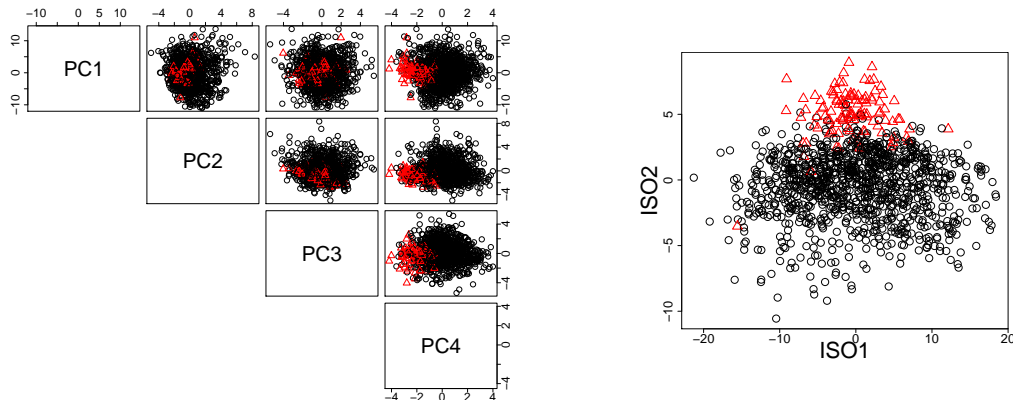


Figure 4: Comparison of gene expression dimension reduction using PCA (left) and Isomap (right) for genes in the Type I diabetes mellitus pathway. Black circles represent TCGA breast cancer tumor tissue and red triangles represent adjacent-normal. Plotted are the projections of the samples in the first four PCA coordinates (left) and first two Isomap coordinates (right). The Isomap embedding enables separation of the tumor and normal samples not achieved by PCA, suggesting that a non-linear pattern of gene expression within the pathway distinguishes tumor and normal samples.

This example motivates the choice of nonlinear dimension reduction as a means of quantifying the overall behavior of a pathway.

2.2.2 Isomap parameter choice

Isomap has one free parameter, k , which defines the k -nearest neighbors used in reconstructing the local geometry [35]. Choosing the optimal value of k is an open question, and different values have the potential to produce different embeddings. We devised a data-driven method for selecting k by employing a comparison between the spectra of PCA and Isomap.

Isomap applies MDS [43] on a distance matrix that approximates geodesic distances, constructed by a k -nearest neighbors search and computing shortest paths. This may be thought of as a localized form of MDS (or, equivalently, PCA [43]), which classically uses distances between all pairs to articulate the global geometry. Like PCA and MDS, Isomap also yields a spectrum of eigenvalues whose magnitude indicates the proportion of variability in the data that is articulated by the corresponding coordinate.

We capitalize on this feature by comparing the spectra of PCA and ISOMAP for different values of k . Spectral comparisons can help find embeddings most different from each other, and may reveal those that articulate manifolds with nonlinear structures. In PCA, one chooses the number of components to be retained such that the majority of the variance in the data is captured. A common visualization is the “scree plot” in which the variance for each component (eigenvalues $\lambda_0 \geq \lambda_1, \geq \dots \geq \lambda_n$) is displayed; one looks for an elbow in the spectrum indicating that additional components do not appreciably reduce the residual variance. Mathematically, an elbow at the first component will have a large ratio between the first two eigengaps (i.e., a large change between the first and second eigenvalues, followed by a much smaller change between the second and third), which we call the spectral gap ratio (SGR), $SGR = \frac{\lambda_0 - \lambda_1}{\lambda_1 - \lambda_2}$.

We choose Isomap k such that it maximizes the SGR ratio between Isomap and PCA, $\frac{SGR_{ISOMAP}}{SGR_{PCA}}$, noting that when $k = N - 1$ (all data treated as nearest-neighbors), Isomap and PCA yield equivalent spectra. The optimal k is guaranteed to yield $\frac{SGR_{ISOMAP}}{SGR_{PCA}} \geq 1$; that is, it produces an embedding that explains at least as much variance in the first component as PCA. By choosing k to maximize this ratio, we obtain the greatest improvement by Isomap over PCA, which will occur when the data lie on a curved manifold that cannot be articulated by PCA.

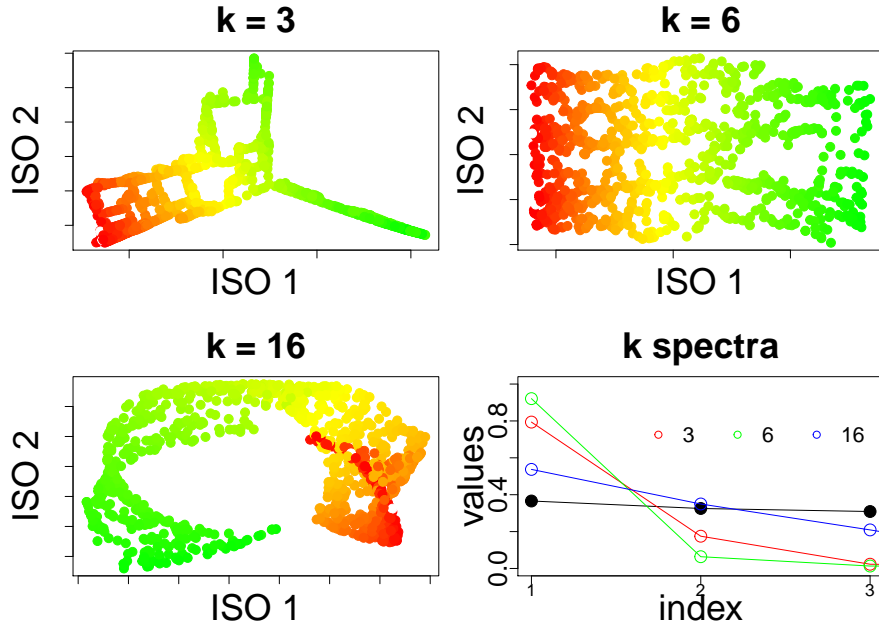


Figure 5: Two-dimensional embedding of the Swiss roll using Isomap for different k values. The bottom right plot shows the spectra using PCA (black dots), and for $k = 3$ (red), $k = 6$ (green), and $k = 16$ (blue) using Isomap. Our “optimal” k ’s spectra, $k = 6$, is most different than PCA’s spectra, as computed by the SGR ratio defined in the methods section.

To illustrate our methodology, we apply Isomap to the Swiss roll dataset using different values of k in Figure 5. The “optimal” k ($k = 6$) produces an embedding that reflects the low-dimensional intrinsic geometry of the roll, the unraveled 2D surface. In comparison, a value is that is too small ($k = 3$) will be sensitive to local distortions, whereas a value that is too large ($k = 16$) will produce an embedding that poorly learns the intrinsic coordinates. The spectra for all three Isomap embeddings, in addition to the PCA spectrum, are shown in the right-most plot in Figure 5. The green empty circles, corresponding to ($k = 6$), have the largest $\frac{SGR_{ISOMAP}}{SGR_{PCA}}$, whereas other k ’s have smaller SGR as shown by the red ($k = 3$) and blue ($k = 16$) empty circles. The “optimal” k produces a PAS that captures the geodesic of the Swiss roll. We applied this methodology to pathway data such that the PAS best represents the geometry of the data in the high-dimensional space.

2.2.3 PAS correlation with miRNAs

Once the PAS is computed, correlations between each pathway’s PAS with each miRNA’s expression are computed class-conditionally. miRNA–pathway correlation differences ($\Delta\rho$) are computed between tumor and adjacent-normal tissue samples as shown in Equation 1. We emphasize that the PAS is computed class-inclusively (both tumor and adjacent-normal tissue) so that different phenotypes are summarized in context with each other. Thus, we can compare phenotypes on the same scale and quantify their gene expression differences across the pathway. Afterwards, we restrict samples to each phenotype and compute their correlation with miRNAs class-conditionally. This enables us to compare how the relationship between a miRNA and a pathway differs in tumor and normal tissue.

The significance of each $\Delta\rho$ is assessed by permutation tests. Each miRNA–pathway pair’s $\Delta\rho$ null distribution is estimated by randomly permuting class labels and recomputing $\Delta\rho$ for 10^5 resamplings. Within each resampling, the same number of nominal tumor and adjacent-normal samples is preserved.

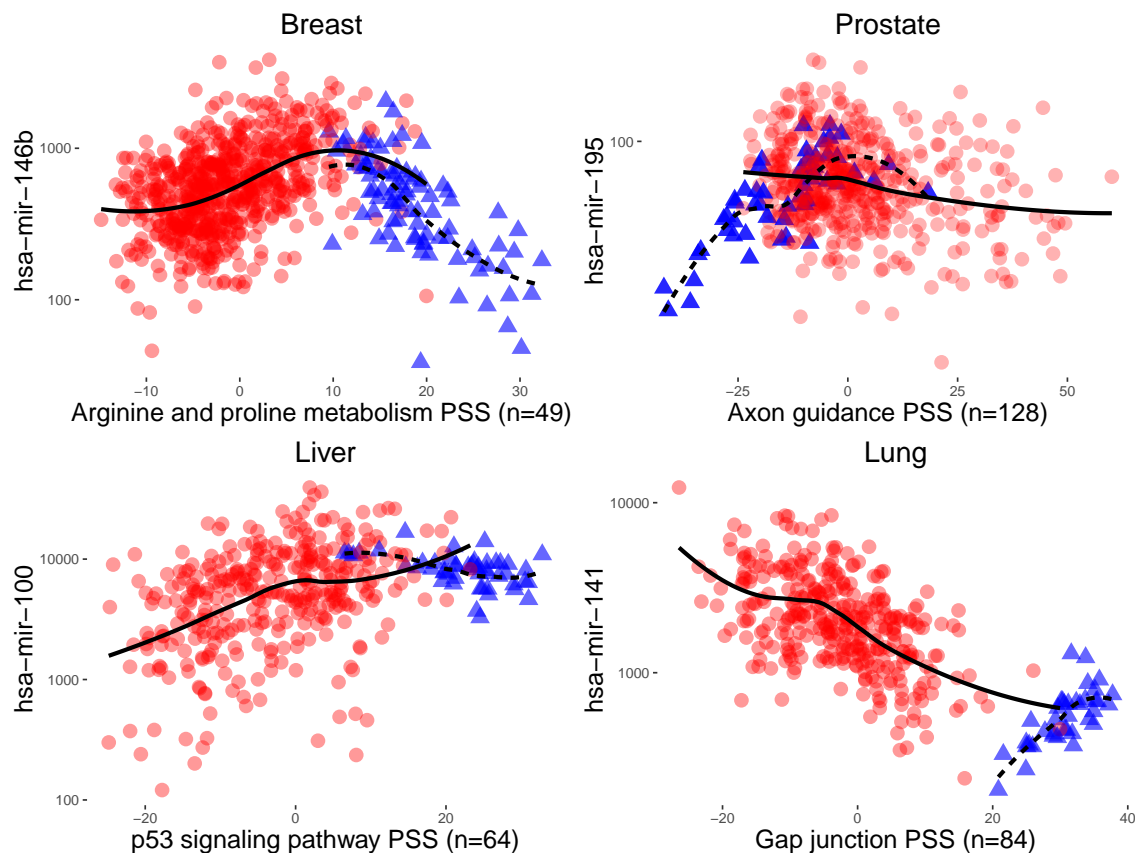


Figure 6: Representative examples of significant miRNA–pathway pairs for all four cancers. miRNA–pathway pairs with the largest $\Delta\rho$ are shown for each cancer ($p < 10^{-5}$). Tumor samples are represented by red circles and adjacent-normal samples by blue triangles. LOESS curves are overlaid by tissue type (solid line for tumor tissue, dotted line for adjacent-normal tissue) to visualize correlation differences. The number of genes in the pathway which have been used in the computation of the PAS are shown in parenthesis.

Adjustment for the multiple hypotheses tested is also achieved through permutation [44].

3 Results

miRNAs with median expression above 0.001 (444 in breast, 455 in liver, 484 in lung, and 416 in prostate) and pathways with greater than five genes (223 pathways) were considered. Each possible miRNA–pathway pair ($\sim 10^5$ pairs) was analyzed for differential association between tumor and adjacent-normal tissue within each organ (breast, prostate, lung, and liver) by computing its $\Delta\rho$ and assessing $\Delta\rho$ significance to identify organ-specific relationships between miRNAs and pathways that appear to be strongly altered in tumors. Multiple hypothesis correction was achieved through permutation [44].

We illustrate aberrant miRNA regulation of pathways in tumor tissue by showing sample miRNA vs. PAS expression plots which have the most pronounced class-correlation differences (Figure 6). In the plots, tumor samples exhibit distinct trends from adjacent-normal samples for the same miRNA and pathway in the same organ.

In these particular cases, the PAS alone can distinguish phenotypes, as demonstrated by the difference in the location of the tumor and normal samples along the x -axes. However, we emphasize that differential

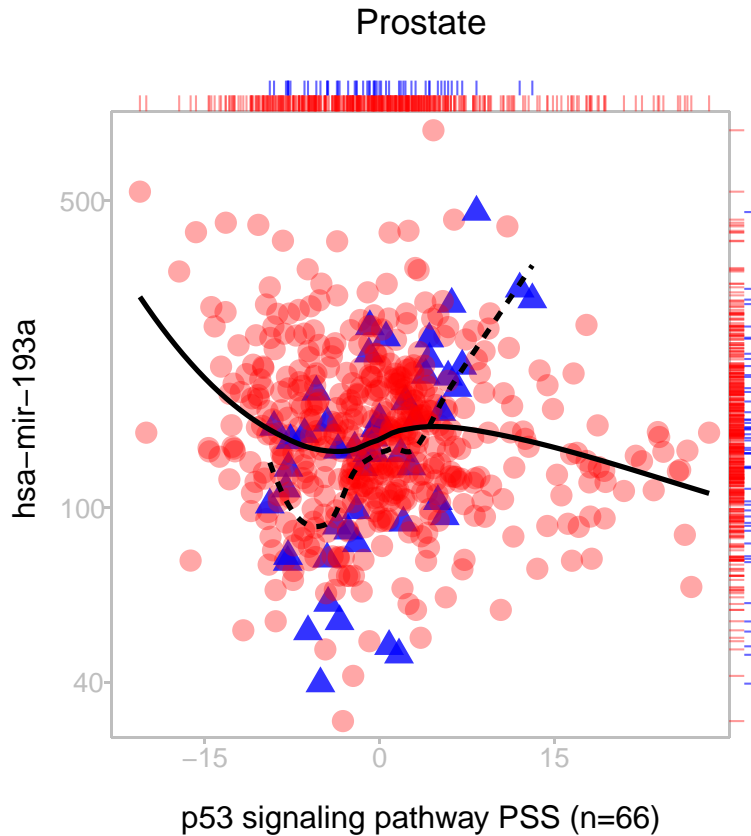


Figure 7: Example of a miRNA–pathway pair (miRNA ID: hsa-mir-193a, KEGG pathway ID: 04115) with significant $\Delta\rho$ ($\Delta\rho = -0.64$, $p < 10^{-4}$) despite no differential expression in prostate cancer. Absence of differential expression is visualized by a rug plot on the top and right. Our method is capable of articulating significant miRNA–pathway coregulation differences regardless of differential expression across either the pathway or miRNA.

Table 2: Top breast cancer pairs sorted by the most pronounced $\Delta\rho$ ($p < 10^{-5}$). ρ_T and ρ_N are the within-tissue Spearman’s rank correlation for tumor tissue and normal tissue, respectively. Size denotes the number of genes in the pathway that have been used in the computation of the the PAS. Targets denotes the number of predicted targets of the miRNA on those genes using TargetScan [48]. In parenthesis, the total number of genes and targets of the miRNA on the pathway are shown.

miRNA	KEGG ID	KEGG name	$\Delta\rho$	ρ_T	ρ_N	size	targets
hsa-mir-146b	00330	Arginine and proline metabolism	1.15	0.44	-0.71	49(54)	1(1)
hsa-mir-146b	05110	Vibrio cholerae infection	1.12	0.44	-0.68	51(54)	0(0)
hsa-mir-146b	05217	Basal cell carcinoma	1.11	0.45	-0.66	53(55)	1(1)
hsa-mir-146b	05200	Pathways in cancer	-1.10	-0.49	0.61	316(326)	10(10)
hsa-mir-135b	00980	Metabolism of xenobiotics by cytochrome P450	1.10	0.48	-0.63	49(71)	0(0)
hsa-mir-146b	05120	Epithelial cell signaling in Helicobacter pylori infection	1.10	0.47	-0.63	66(68)	0(0)
hsa-mir-135b	05217	Basal cell carcinoma	1.08	0.48	-0.60	53(55)	5(5)
hsa-mir-146b	00980	Metabolism of xenobiotics by cytochrome P450	1.08	0.46	-0.61	49(71)	0(0)
hsa-mir-99a	00590	Arachidonic acid metabolism	1.07	0.49	-0.58	48(59)	0(0)
hsa-mir-135b	00520	Amino sugar and nucleotide sugar metabolism	1.07	0.44	-0.63	47(48)	0(0)
hsa-mir-1307	00830	Retinol metabolism	-1.07	-0.51	0.56	42(64)	0(0)
hsa-mir-1307	04976	Bile secretion	-1.06	-0.61	0.45	56(71)	0(0)
hsa-mir-135b	00051	Fructose and mannose metabolism	1.06	0.44	-0.63	35(36)	1(1)
hsa-mir-135b	05120	Epithelial cell signaling in Helicobacter pylori infection	1.06	0.41	-0.65	66(68)	4(4)
hsa-mir-224	01040	Biosynthesis of unsaturated fatty acids	1.06	0.40	-0.65	19(21)	0(0)

expression within a pathway is unnecessary for achieving significance. Our method also detects aberrant signaling even when no marginal differences can be detected. Figure 7 shows a sample miRNA vs. pathway expression plot in prostate cancer with a significant correlation change despite a lack of differential expression across either the PAS or miRNA. Such a pair would not be detected using methods which rely on single gene association statistics, or by looking at the pathway in isolation without the miRNA.

Importantly, other evidence from the literature supports the association of this miRNA–pathway pair. The miRNA in Figure 7, hsa-mir-193a, is a tumor suppressor implicated in several cancers whose down-regulation has been proposed as a biomarker of oncogenesis [45, 27, 46]. The p53 signaling pathway, a tumor suppressing pathway which responds to cell stress, can activate cell cycle arrest, senescence, or apoptosis. It is known as a prominent regulator which is commonly disrupted in cancer cells [47], and its main tumor protein TP53 is the most mutated gene in cancer. In addition, the p53 pathway contains three genes which are predicted to be targets of hsa-mir-193a (CCND1, SIAH1, and ZMAT3). This example serves to illustrate the capabilities of the method to detect biologically meaningful relationships between miRNA expression and pathway activity.

In the following sections, we list the top 15 pairs with the most pronounced $\Delta\rho$ for each cancer type. The remaining pairs at the same level of significance are listed in the Supplementary Information. Many of the flagged miRNAs and pathways have a biological basis for disruption in cancer.

3.1 Breast Cancer

Breast cancer pairs with large $\Delta\rho$ are shown in Table 2. miRNAs hsa-mir-146b and hsa-mir-135b each regulate multiple pathways class-conditionally and have functional relevance to cancer in the literature. Specifically, hsa-mir-146b is a known tumor suppressor [49, 50] that inhibits NF- κ B induction of IL-6 to prevent inflammation in breast cells, which chronically leads to oncogenesis. In breast cancer cells, however, promoter methylation decreases hsa-mir-146b expression [51]. hsa-mir-135b has previously been associated with several cancer types, including prostate, lung, and most prominently colon cancer. In colon cancer,

upregulation of hsa-mir-135b promotes cancer progression, and activation of hsa-mir-135b is triggered by oncogenic pathways [52]. The IL-1R1 pathway, which involves regulation of immune and inflammatory responses, has recently been found to regulate hsa-mir-135b expression in smoke-induced inflammation in lung cells [53].

It is notable that several pathways which are listed, including those differentially regulated by hsa-mir-146b and hsa-mir-135b, are inflammatory. Infectious disease pathways, including *Vibrio cholerae* infection and Epithelial cell signaling in *Helicobacter pylori* infection, activate proinflammatory responses including the upregulation of various inflammatory cytokines after infection. Cytochrome P450, the main enzyme in Metabolism of xenobiotics by cytochrome P450, is regulated by several inflammatory mediators and its expression and activity is decreased with a host response to inflammation and infection [54].

These miRNAs and pathways are of interest because chronic inflammation is broadly associated with tumorigenesis and cancer. Chronic inflammation has been shown to increase the risk of tumor formation, notably demonstrated in the association between chronic inflammatory bowel disease and colon carcinogenesis. Inflammatory mediators and inflammation in the tumor microenvironment have many cancer-promoting effects including promotion of malignant cells, angiogenesis, subversion of immune responses, metastasis, induction of proneoplastic mutations, and altered response to hormones [55, 56, 57]. Proinflammatory chemokines and cytokines have been found in the tumor microenvironment of many cancers and are typically induced by hypoxic conditions, which are characteristic of tumors [58].

In addition, several metabolic pathways are represented. Arginine and proline metabolism has been known to exhibit changes in cancer [59], and the proline regulatory axis and proline metabolism both undergo alterations that are posited to sustain and promote tumor cell growth [60, 61]. A plot of hsa-mir-146b differentially regulating Arginine and proline metabolism is shown in Figure 6. Interestingly, two cancer pathways (Pathways in Cancer and Basal Cell Carcinoma) contain the most predicted miRNA targets, including cancer genes NRAS, CCDC6, CSF1R, SMAD4, ITGAV, and several others. However, it should be noted that many miRNA–pathway pairs contain no predicted miRNA targets. Sequence matching using TargetScan will fail to capture indirect interactions between miRNAs and pathway genes that may indeed be captured using correlations. For instance, the IL-1R receptor family, which regulates hsa-mir-135b expression (see above), activates cytokines IL-6 and IL-8 which are present or interact with multiple inflammatory pathways in Table 2, even though they are not predicted targets of hsa-mir-135b.

3.2 Prostate Cancer

hsa-mir-195 is flagged with many pathways in prostate cancer, shown in Table 3. hsa-mir-195 is frequently reported as deleted or downregulated in tumors across multiple cancer types [62, 63, 64]. In prostate cancer hsa-mir-195 is under-expressed and has been shown to behave as a tumor suppressor by regulating RPS6KB1 [65], BCOX1 [66], and FGF2 [67]. hsa-mir-195 itself is part of the hsa-mir-15 family cluster, whose hsa-mir-15a has also been shown to behave as a tumor suppressor by regulating oncogenes BCL2, CCND1 and WNT3 [68]. In advanced prostate tumors, hsa-mir-15a is downregulated or deleted and these oncogene levels are markedly increased. Relatedly, the loss of the hsa-mir-15 family in prostate cancer has been found to contribute to metastatic potential including bone lesions [69] (a marker of metastasis).

Many oncogenes are regulated by hsa-mir-195, including BCL2, CCND1, WNT3, AKT3, CDC42, RAF1, and KRAS that lie on the pathways flagged with hsa-mir-195 in Table 3. These pathways include two cancer pathways (Melanoma and Basal cell carcinoma), morphological pathways (Axon guidance and Focal adhesion), and several signaling pathways whose genes are expected to be altered in tumors. Interestingly, most miRNA–pathway pairs in Table 3, and particularly those with hsa-mir-195, exhibit much stronger correlations in normal samples than in tumor samples. These trends may indicate general loss of function in tumorigenesis, in concordance with documented under-expression of hsa-mir-195 in tumors.

Table 3: Top prostate cancer pairs sorted by the most pronounced $\Delta\rho$ ($p < 10^{-5}$).

miRNA	KEGG ID	KEGG name	$\Delta\rho$	ρ_T	ρ_N	size	targets
hsa-mir-195	04360	Axon guidance	-0.93	-0.19	0.75	128(129)	16(17)
hsa-mir-195	04510	Focal adhesion	0.88	0.18	-0.70	194(200)	30(31)
hsa-mir-195	05218	Melanoma	0.88	0.18	-0.70	63(71)	16(16)
hsa-mir-1307	05410	Hypertrophic cardiomyopathy (HCM)	0.86	0.38	-0.49	75(83)	0(0)
hsa-mir-195	05217	Basal cell carcinoma	-0.85	-0.17	0.68	54(55)	10(10)
hsa-mir-1307	05414	Dilated cardiomyopathy	-0.85	-0.39	0.46	81(90)	0(0)
hsa-mir-1307	04122	Sulfur relay system	-0.85	-0.23	0.62	10(10)	0(0)
hsa-mir-200a	03022	Basal transcription factors	-0.84	-0.17	0.68	35(36)	0(0)
hsa-mir-944	00982	Drug metabolism - cytochrome P450	-0.83	-0.52	0.32	55(73)	0(0)
hsa-mir-141	00592	alpha-Linolenic acid metabolism	0.83	0.42	-0.42	16(20)	0(0)
hsa-mir-195	04964	Proximal tubule bicarbonate reclamation	0.83	0.15	-0.67	22(23)	3(4)
hsa-mir-195	04912	GnRH signaling pathway	0.83	0.13	-0.70	92(101)	10(10)
hsa-mir-195	05414	Dilated cardiomyopathy	0.82	0.14	-0.69	81(90)	5(5)
hsa-mir-195	04664	Fc epsilon RI signaling pathway	0.82	0.14	-0.69	70(79)	10(10)
hsa-mir-195	05100	Bacterial invasion of epithelial cells	0.82	0.20	-0.62	69(70)	5(5)

Table 4: Top liver cancer pairs sorted by the most pronounced $\Delta\rho$ ($p < 10^{-5}$).

miRNA	KEGG ID	KEGG name	$\Delta\rho$	ρ_T	ρ_N	size	targets
hsa-mir-100	04115	p53 signaling pathway	0.85	0.38	-0.47	64(68)	0(0)
hsa-mir-3607	04320	Dorso-ventral axis formation	0.82	0.26	-0.56	20(24)	0(0)
hsa-mir-34a	04115	p53 signaling pathway	0.81	0.29	-0.53	64(68)	8(8)
hsa-mir-100	00360	Phenylalanine metabolism	0.81	0.53	-0.28	17(17)	0(0)
hsa-mir-210	03030	DNA replication	-0.81	-0.45	0.36	36(36)	0(0)
hsa-mir-210	05219	Bladder cancer	-0.81	-0.41	0.40	41(42)	0(0)
hsa-mir-210	05322	Systemic lupus erythematosus	-0.81	-0.35	0.46	103(136)	0(0)
hsa-mir-210	04110	Cell cycle	-0.81	-0.42	0.38	117(124)	0(0)
hsa-mir-148b	04614	Renin-angiotensin system	0.80	0.19	-0.61	14(17)	1(1)
hsa-mir-139	00053	Ascorbate and aldarate metabolism	-0.80	-0.36	0.45	24(26)	0(0)
hsa-mir-34a	00620	Pyruvate metabolism	0.80	0.29	-0.51	37(40)	1(1)
hsa-mir-34a	00591	Linoleic acid metabolism	0.80	0.32	-0.47	23(30)	0(0)
hsa-mir-1247	00460	Cyanoamino acid metabolism	-0.80	-0.46	0.34	7(7)	0(0)
hsa-mir-100	00983	Drug metabolism - other enzymes	0.79	0.56	-0.24	49(52)	0(0)
hsa-mir-139	00330	Arginine and proline metabolism	0.78	0.58	-0.20	51(54)	2(2)

3.3 Liver Cancer

In Table 4, flagged pairs for liver cancer are shown. miRNAs hsa-mir-100, hsa-mir-34a, and hsa-mir-210 are represented several times and are each known to be involved in hepatocellular carcinoma. hsa-mir-100 downregulation, concomitant with increased expression of its target PLK1, correlates with poor prognosis and is an early event in hepatocarcinogenesis [70, 71]. Several studies have shown hsa-mir-34a to be a tumor suppressor that activates apoptosis and cell senescence. In hepatocellular carcinoma, hsa-mir-34a suppresses tumor invasion by modulating c-Met expression and is typically underexpressed [72, 73]. In addition, hsa-mir-210 upregulation is increased in hypoxic conditions and contributes to metastatic potential in hepatocellular carcinoma [74].

hsa-mir-100 and hsa-mir-34a are both found to differentially regulate the p53 signaling pathway in Table 4. This is of interest because p53 is very commonly implicated in cancer, and in liver cancer, p53 loss is associated with aggressive carcinomas and restoration of p53 has been shown to initiate tumor regression [75]. Notably, hsa-mir-34a and hsa-mir-34 family members are part of the p53 transcriptional network

Table 5: Top lung cancer pairs sorted by the most pronounced $\Delta\rho$ ($p < 10^{-5}$).

miRNA	KEGG ID	KEGG name	$\Delta\rho$	ρ_T	ρ_N	size	targets
hsa-mir-141	04540	Gap junction	-1.26	-0.52	0.74	84(90)	8(8)
hsa-mir-141	05146	Amoebiasis	1.19	0.54	-0.65	102(106)	5(5)
hsa-mir-203	04530	Tight junction	1.13	0.44	-0.69	121(132)	14(14)
hsa-mir-141	05100	Bacterial invasion of epithelial cells	-1.13	-0.55	0.58	68(70)	5(5)
hsa-mir-141	04510	Focal adhesion	1.11	0.55	-0.56	195(200)	8(8)
hsa-mir-141	04916	Melanogenesis	-1.11	-0.45	0.66	98(101)	5(5)
hsa-mir-141	04670	Leukocyte transendothelial migration	1.10	0.57	-0.53	109(116)	2(2)
hsa-mir-141	04974	Protein digestion and absorption	-1.09	-0.53	0.56	70(81)	3(3)
hsa-mir-150	04973	Carbohydrate digestion and absorption	1.08	0.52	-0.56	35(44)	1(1)
hsa-mir-222	05146	Amoebiasis	1.07	0.43	-0.64	102(106)	1(1)
hsa-mir-141	05200	Pathways in cancer	1.06	0.53	-0.53	315(326)	25(25)
hsa-mir-150	04660	T cell receptor signaling pathway	-1.05	-0.62	0.43	103(108)	4(4)
hsa-mir-200c	04540	Gap junction	-1.05	-0.39	0.66	84(90)	13(13)
hsa-mir-141	04145	Phagosome	1.05	0.54	-0.51	142(153)	6(6)
hsa-mir-141	00260	Glycine, serine and threonine metabolism	-1.04	-0.44	0.60	29(32)	0(0)

and are directly regulated by p53 [76, 77]. p53 induces the transcription of the hsa-mir-34 family, which downregulates CDK4 and CDK6 to induce cell cycle arrest and BCL2 to promote apoptosis [78]. hsa-mir-34a itself is predicted to directly regulate 8 targets on the p53 signaling pathway, including tumor-associated genes CCND1, CCNE2, TP73, and CDK6. In addition, p53 induces the transcription of other miRNAs (hsa-mir-145, hsa-mir-192/215, and hsa-mir-107) that modulate genes to induce cell cycle arrest, reduce cell proliferation, and suppress angiogenesis [78].

3.4 Lung Cancer

Flagged pairs in lung cancer are shown in Table 5. hsa-mir-141 is represented frequently and is part of a miRNA family containing five members arranged as two clusters, hsa-mir-200a/200b/429 and hsa-mir-141/200c, that is thought to suppress the epithelial to mesenchymal transition (EMT). This is of interest because the EMT is believed to be an important step in metastasis. The EMT is marked by decreased cell adhesions including repression of E-cadherin and increased cell motility. This miRNA family has been observed to play a role in the EMT of many cancer types, including bladder, breast, melanoma, prostate, and lung cancer. In lung cancer, it has been shown to suppress the EMT with forced increased expression, while EMT was observed in lung cancer cells with low expression of hsa-mir-200 [79]. In addition, hsa-mir-141 has been shown to be a prognostic indicator in lung cancer [80] and promotes proliferation by targeting PHLPP1 and PHLPP2 [81].

It is notable that many of the pathways in Table 5 are morphological and dictate cellular processes remodeled during the EMT. Gap junctions, Tight junctions, and Focal adhesions all undergo significant changes to decrease cell-cell adhesions and promote invasion. In Table 5, miRNAs hsa-mir-141 and hsa-mir-200c both differentially regulate Gap junctions (hsa-mir-141 vs. Gap junction PAS is shown in Figure 6). Diminished Gap junctions or their elimination are seen as important indicators of tumorigenesis [82, 83]. In addition, many cancer genes targeted by hsa-mir-141 and its family members are on the pathways in Table 5, including SRC, PTEN, GRB2, CDK6, KRAS, DCC, and various protein kinases. These genes are reported to play significant roles in multiple cancers in the literature.

3.5 Pathway miRNA targets

It is reasonable to ask whether the associations detected between miRNAs and pathways are driven by an abundance of targetted genes on those pathways. Tables 2–5 list the number of genes on the pathway that are targetted by the associated miRNA. As noted above, several pathways do contain multiple targets of a miRNA. However, we detect many more pathways that exhibit a differential association with a miRNA despite the fact that the pathways are not known to contain miRNA targets. To address this question systematically, we tested whether an abundance of miRNA targets in a pathway was predictive of a strong association in the analysis above. Briefly, we were unable to detect any relationship between the strength of the differential miRNA–pathway association and the proportion of miRNA targets on the pathway. Further details may be found in the Supplementary Information.

4 Discussion

We have described a new method for integrating miRNA and gene expression data to elucidate the role of miRNAs in regulating functional pathways and identifying miRNA–pathway pairs whose co-regulation may be disrupted in cancer.

Our approach improves upon other methods that have recently been proposed to study miRNA regulation of pathways in cancer. Many of these approaches rely on miRNA target prediction coupled with enrichment analyses. For instance, [84] identified prognostic miRNAs based on survival analysis and then used functional network analysis to identify potential pathways regulated by those miRNAs using gene ontology terms, and [85] developed GSEA-FAME to infer miRNA activity from mRNA expression data using enrichment and weighted miRNA–mRNA interaction methods. Both methods have been applied to TCGA data in order to identify biomarkers and interpret miRNA function in cancer. However, functional enrichment has been shown to contain bias [86], and commonly used *in silico* approaches tend to identify highly related biological processes [40]. In addition, these methods typically ignore context dependent changes in miRNA regulation; it is well known that miRNAs exhibit heterogeneous effects across cell, tissue, and tumor types.

In contrast, our method does not rely on miRNA target prediction and functional enrichment, avoiding those sources of bias. Rather, our approach is fully data driven, integrating sample specific miRNA and mRNA expression data for identifying miRNA–pathway regulation. This takes into account any context dependent behavior of miRNAs, since miRNA and mRNA expression are compared using the same biological samples. By summarizing the gene expression behavior on the pathway with the PAS instead of performing enrichment analysis, we capture the overall effect of the miRNA on the pathway, avoiding the bias introduced by correlated genes [86]. The use of nonlinear dimension reduction to obtain the PAS also enables this method to articulate complex coregulatory dynamics (such as that illustrated in Fig. 1). By comparing the miRNA–pathway relationship in tumor tissue to that in adjacent normal tissue, the method is able to identify regulatory relationships which are disrupted in disease. Other methods typically focus only on tumor tissue and therefore cannot distinguish regulation uniquely affected in tumors.

Our pathway summary compresses high dimensional expression of all constitutive genes using samples of both phenotypes in the same organ. Because it computes the summary collectively, in the context of all other genes and samples, it does not rely on independent statistical associations with the phenotype of interest. Importantly, this approach takes into account systemic effects and has the ability to articulate nonlinear geometries, which may separate out phenotypes even if their boundaries are not convex. Class-conditional correlations of the pathway summaries with miRNA expression between phenotypes can identify aberrantly regulated miRNA–pathway relationships even in the absence of differential expression across either the miRNA or pathway. This is in contrast to other approaches which rely on individual differential expression of miRNAs or genes to detect systemic differences across phenotypes. The use of pathways,

rather than individual genes, significantly reduces the search space of relevant processes while increasing interpretability.

We integrate sample-specific miRNA and mRNA expression data from TCGA and compare tumor to adjacent-normal tissue samples from breast, prostate, liver, and lung cancers. We find that within each cancer type, more miRNA–pathway relationships are aberrantly regulated in tumors than expected by chance. This supports the notion that complex diseases like cancer contain perturbations to entire systems rather than to a few individual genes. Additionally, many of the flagged miRNAs and pathways have a biological basis for disruption in cancer. We find specific relationships related to inflammatory processes, EMT modulation, and tumor suppression (p53 signaling) that are highly perturbed in tumors. Comparison of results across cancer types exhibited differences in the miRNA–pathway pairs detected, suggesting that the underlying molecular mechanisms differ across tissues.

Because our method relies on statistical associations of expression data, it does not incorporate known miRNA–gene target relationships *a priori*. To investigate whether our findings of significant miRNA–pathway pairs were driven by an abundance of miRNA targets on the pathway, we tested whether flagged miRNA–pathway pairs were more likely to be enriched with predicted miRNA targets, and found poor association in all cancer types (see Supplementary Information). We found no association between the significance of the miRNA–pathway results and the number of miRNA target genes on the pathway, suggesting that indirect coregulation of the miRNA and the pathway genes contributes to our results. Notably, the significance of many miRNA–pathway pairs would be missed using methods that rely on miRNA target lists to identify miRNA-regulated pathways. Other potential artifacts that could influence significance, such as miRNA differential expression and pathway size, also showed little association with our findings (see Supplementary Information), suggesting that these too are not driving our findings. Together, this supports the view that the method is capable of detecting biologically significant miRNA–pathway relationships at the systems level that either cause or emerge from a phenotype change, and which may be missed using other approaches.

Finally, while we apply our algorithm to miRNA and gene expression data in cancer, we note that it can be generalized to other experimental modalities and diseases, provided sufficient data for cases and controls. Future applications could include other regulatory mechanisms such as transcription factors, epigenetic modifications, or small molecule inhibitors. In addition, other complex diseases could be investigated that are thought to undergo significant perturbations at the systems level. Identifying altered associations at the systems level helps narrow down the search space for responsible mechanisms that contribute to tumorigenesis.

5 Acknowledgements

The authors wish to thank Sara Solla for helpful suggestions.

6 Funding

National Institutes of Health (5K22CA148779 to RB); J.S.McDonnell Foundation (to RB); Northwestern University Data Science Initiative (to GW and RB).

6.0.1 Conflict of interest statement.

None declared.

References

- [1] Victor Ambros. The functions of animal microRNAs. *Nature*, 431(7006):350–355, 2004.
- [2] Benjamin P Lewis, Christopher B Burge, and David P Bartel. Conserved seed pairing, often flanked by adenosines, indicates that thousands of human genes are microRNA targets. *Cell*, 120(1):15–20, 2005.
- [3] Sam Griffiths-Jones, Harpreet Kaur Saini, Stijn van Dongen, and Anton J Enright. miRBase: tools for microRNA genomics. *Nucleic Acids Research*, 36(suppl_1):D154–D158, 2007.
- [4] Robin C Friedman, Kyle Kai-How Farh, Christopher B Burge, and David P Bartel. Most mammalian mRNAs are conserved targets of microRNAs. *Genome research*, 19(1):92–105, 2009.
- [5] Sung Wook Chi, Gregory J Hannon, and Robert B Darnell. An alternative mode of microRNA target recognition. *Nature Structural & Molecular Biology*, 19(3):321–327, 2012.
- [6] Qinghua Cui, Zhenbao Yu, Enrico O Purisima, and Edwin Wang. Principles of microRNA regulation of a human cellular signaling network. *Molecular Systems Biology*, 2(1), 2006.
- [7] Stephan Artmann, Klaus Jung, Annalen Bleckmann, and Tim Beißbarth. Detection of simultaneous group effects in microRNA expression and related target gene sets. *PLoS One*, 7(6):e38365, 2012.
- [8] Chengxiang Qiu, Juan Wang, Pengying Yao, Edwin Wang, and Qinghua Cui. microRNA evolution in a human transcription factor and microRNA regulatory network. *BMC Systems Biology*, 4(1):90, 2010.
- [9] Wan Hee Yoon, Hans Meinhardt, and Denise J Montell. miRNA-mediated feedback inhibition of JAK/STAT morphogen signalling establishes a cell fate threshold. *Nature Cell Biology*, 13(9):1062–1069, 2011.
- [10] Wei Zhu and Yi-Ping Phoebe Chen. Computational developments in microRNA-regulated protein-protein interactions. *BMC Systems Biology*, 8(1):14, 2014.
- [11] Thalia A Farazi, Jessica I Spitzer, Pavel Morozov, and Thomas Tuschl. miRNAs in human cancer. *The Journal of Pathology*, 223(2):102–115, 2011.
- [12] Thales Papagiannakopoulos, Alice Shapiro, and Kenneth S Kosik. MicroRNA-21 targets a network of key tumor-suppressive pathways in glioblastoma cells. *Cancer Research*, 68(19):8164–8172, 2008.
- [13] E Maria C Ohlsson Teague, Kylie H Van der Hoek, Mark B Van der Hoek, Naomi Perry, Prabhath Wagaarachchi, Sarah A Robertson, Cristin G Print, and Louise M Hull. MicroRNA-regulated pathways associated with endometriosis. *Molecular Endocrinology*, 23(2):265–275, 2009.
- [14] Maurizio Ceppi, Patricia M Pereira, Isabelle Dunand-Sauthier, Emmanuèle Barras, Walter Reith, Manuel A Santos, and Philippe Pierre. MicroRNA-155 modulates the interleukin-1 signaling pathway in activated human monocyte-derived dendritic cells. *Proceedings of the National Academy of Sciences*, 106(8):2735–2740, 2009.
- [15] Christopher J Walsh, Pingzhao Hu, Jane Batt, and Claudia C dos Santos. Discovering microRNA-regulatory modules in multi-dimensional cancer genomic data: a survey of computational methods. *Cancer Informatics*, 15(Suppl 2):25, 2016.

- [16] Jihong Fu, Wentao Tang, Peng Du, Guanghui Wang, Wei Chen, Jingming Li, Yunxiang Zhu, Jun Gao, and Long Cui. Identifying microRNA–mRNA regulatory network in colorectal cancer by a combination of expression profile and bioinformatics analysis. *BMC systems biology*, 6(1):68, 2012.
- [17] Yue Li, Cheng Liang, Ka-Chun Wong, Jiawei Luo, and Zhaolei Zhang. Mirsynergy: detecting synergistic miRNA regulatory modules by overlapping neighbourhood expansion. *Bioinformatics*, 30(18):2627–2635, 2014.
- [18] Xiaowei Chen, Frank J Slack, and Hongyu Zhao. Joint analysis of expression profiles from multiple cancers improves the identification of microRNA–gene interactions. *Bioinformatics*, 29(17):2137–2145, 2013.
- [19] Thuc Duy Le, Junpeng Zhang, Lin Liu, and Jiuyong Li. Ensemble methods for miRNA target prediction from expression data. *PloS One*, 10(6):e0131627, 2015.
- [20] Vessela N Kristensen, Ole Christian Lingjærde, Hege G Russnes, Hans Kristian M Volla, Arnaldo Frigessi, and Anne-Lise Børresen-Dale. Principles and methods of integrative genomic analyses in cancer. *Nature Reviews Cancer*, 14(5):299–313, 2014.
- [21] Yingying Wei. Integrative analyses of cancer data: a review from a statistical perspective. *Cancer Informatics*, 14(Suppl 2):173, 2015.
- [22] Zi Yang and George Michailidis. A non-negative matrix factorization method for detecting modules in heterogeneous omics multi-modal data. *Bioinformatics*, 32(1):1–8, 2015.
- [23] Dokyoon Kim, Ruowang Li, Scott M Dudek, and Marylyn D Ritchie. Predicting censored survival data based on the interactions between meta-dimensional omics data in breast cancer. *Journal of Biomedical Informatics*, 56:220–228, 2015.
- [24] Minoru Kanehisa and Susumu Goto. KEGG: Kyoto encyclopedia of genes and genomes. *Nucleic Acids Research*, 28(1):27–30, 2000.
- [25] Carl F Schaefer, Kira Anthony, Shiva Krupa, Jeffrey Buchoff, Matthew Day, Timo Hannay, and Kenneth H Buetow. PID: the pathway interaction database. *Nucleic Acids Research*, 37(suppl 1):D674–D679, 2009.
- [26] Xinxia Peng, Yu Li, Kathie-Anne Walters, Elizabeth R Rosenzweig, Sharon L Lederer, Lauri D Aicher, Sean Proll, and Michael G Katze. Computational identification of hepatitis C virus associated microRNA–mRNA regulatory modules in human livers. *BMC genomics*, 10(1):373, 2009.
- [27] Stefan Uhlmann, Heiko Mannsperger, Jitao David Zhang, Emöke-Ágnes Horvat, Christian Schmidt, Moritz Küblbeck, Frauke Henjes, Aoife Ward, Ulrich Tschulena, Katharina Zweig, et al. Global microRNA level regulation of EGFR-driven cell-cycle protein network in breast cancer. *Molecular Systems Biology*, 8(1):570, 2012.
- [28] Aravind Subramanian, Pablo Tamayo, Vamsi K Mootha, Sayan Mukherjee, Benjamin L Ebert, Michael A Gillette, Amanda Paulovich, Scott L Pomeroy, Todd R Golub, Eric S Lander, et al. Gene set enrichment analysis: a knowledge-based approach for interpreting genome-wide expression profiles. *Proceedings of the National Academy of Sciences of the United States of America*, 102(43):15545–15550, 2005.
- [29] John Tomfohr, Jun Lu, and Thomas B Kepler. Pathway level analysis of gene expression using singular value decomposition. *BMC Bioinformatics*, 6(1):225, 2005.

- [30] Rosemary Braun, Leslie Cope, and Giovanni Parmigiani. Identifying differential correlation in gene/pathway combinations. *BMC Bioinformatics*, 9(1):488, 2008.
- [31] Rosemary Braun, Gregory Leibon, Scott Pauls, and Daniel Rockmore. Partition decoupling for multi-gene analysis of gene expression profiling data. *BMC Bioinformatics*, 12(1):497, 2011.
- [32] Roberto-Rafael Ramos-Rodriguez, Raquel Cuevas-Diaz-Duran, Francesco Falciani, Jose-Gerardo Tamez-Peña, and Victor Trevino. COMPADRE: an R and web resource for pathway activity analysis by component decompositions. *Bioinformatics*, 28(20):2701–2702, 2012.
- [33] Jinlong Shi and Zhigang Luo. Nonlinear dimensionality reduction of gene expression data for visualization and clustering analysis of cancer tissue samples. *Computers in Biology and Medicine*, 40(8):723–732, 2010.
- [34] Mi Hyeon Kim, Hwa Jeong Seo, Je-Gun Joung, and Ju Han Kim. Comprehensive evaluation of matrix factorization methods for the analysis of DNA microarray gene expression data. *BMC Bioinformatics*, 12(13):S8, 2011.
- [35] Joshua B Tenenbaum, Vin De Silva, and John C Langford. A global geometric framework for nonlinear dimensionality reduction. *Science*, 290(5500):2319–2323, 2000.
- [36] The Cancer Genome Atlas Research Network. <http://cancergenome.nih.gov/>, 2005.
- [37] Yue Li, Minggao Liang, and Zhaolei Zhang. Regression analysis of combined gene expression regulation in acute myeloid leukemia. *PLoS Computational Biology*, 10(10):e1003908, 2014.
- [38] George S Krasnov, Alexey A Dmitriev, Nataliya V Melnikova, Andrew R Zaretsky, Tatiana V Nasedkina, Alexander S Zasedatelev, Vera N Senchenko, and Anna V Kudryavtseva. CrossHub: a tool for multi-way analysis of The Cancer Genome Atlas (TCGA) in the context of gene expression regulation mechanisms. *Nucleic Acids Research*, page gkv1478, 2016.
- [39] Chad J Creighton, Anadulce Hernandez-Herrera, Anders Jacobsen, Douglas A Levine, Parminder Mankoo, Nikolaus Schultz, Ying Du, Yiqun Zhang, Erik Larsson, Robert Sheridan, et al. Integrated analyses of microRNAs demonstrate their widespread influence on gene expression in high-grade serous ovarian carcinoma. *PloS One*, 7(3):e34546, 2012.
- [40] Patrice Godard and Jonathan van Eyll. Pathway analysis from lists of microRNAs: common pitfalls and alternative strategy. *Nucleic Acids Research*, page gkv249, 2015.
- [41] Ido Wolf, Siegal Sadetzki, Raphael Catane, Avraham Karasik, and Bella Kaufman. Diabetes mellitus and breast cancer. *Lancet Oncology*, 6(2):103–111, 2005.
- [42] Susanna C Larsson, Christos S Mantzoros, and Alicja Wolk. Diabetes mellitus and risk of breast cancer: a meta-analysis. *International Journal of Cancer*, 121(4):856–862, 2007.
- [43] Trevor F Cox and Michael AA Cox. *Multidimensional Scaling*. CRC Press, 2000.
- [44] Pak C Sham and Shaun M Purcell. Statistical power and significance testing in large-scale genetic studies. *Nature reviews. Genetics*, 15(5):335, 2014.
- [45] Hongwei Liang, Minghui Liu, Xin Yan, Yong Zhou, Wengong Wang, Xueliang Wang, Zheng Fu, Nan Wang, Suyang Zhang, Yanbo Wang, et al. miR-193a-3p functions as a tumor suppressor in lung cancer by down-regulating ERBB4. *Journal of Biological Chemistry*, 290(2):926–940, 2015.

- [46] Peng Zhang, Deng-Bo Ji, Hai-Bo Han, Yun-Fei Shi, Chang-Zheng Du, and Jin Gu. Downregulation of miR-193a-5p correlates with lymph node metastasis and poor prognosis in colorectal cancer. *World Journal of Gastroenterology*, 20(34):12241, 2014.
- [47] Charles J Sherr and Frank McCormick. The RB and p53 pathways in cancer. *Cancer Cell*, 2(2):103–112, 2002.
- [48] Benjamin P Lewis, I-hung Shih, Matthew W Jones-Rhoades, David P Bartel, and Christopher B Burge. Prediction of mammalian microRNA targets. *Cell*, 115(7):787–798, 2003.
- [49] Amandine I Garcia, Monique Buisson, Pascale Bertrand, Ruth Rimokh, Etienne Rouleau, Bernard S Lopez, Rosette Lidereau, Ivan Mikaélian, and Sylvie Mazoyer. Down-regulation of BRCA1 expression by miR-146a and miR-146b-5p in triple negative sporadic breast cancers. *EMBO Molecular Medicine*, 3(5):279–290, 2011.
- [50] D Bhaumik, GK Scott, S Schokrpur, CK Patil, J Campisi, and CC Benz. Expression of microRNA-146 suppresses NF- κ B activity with reduction of metastatic potential in breast cancer cells. *Oncogene*, 27(42):5643–5647, 2008.
- [51] Michael Xiang, Nicolai J Birkbak, Vida Vafaizadeh, Sarah R Walker, Jennifer E Yeh, Suhu Liu, Yasmin Kroll, Mark Boldin, Konstantin Taganov, Bernd Groner, et al. STAT3 induction of miR-146b forms a feedback loop to inhibit the NF- κ B to IL-6 signaling axis and STAT3-driven cancer phenotypes. *Science Signaling*, 7(310):ra11–ra11, 2013.
- [52] Nicola Valeri, Chiara Braconi, Pierluigi Gasparini, Claudio Murgia, Andrea Lampis, Viola Paulus-Hock, Jonathan R Hart, Lynn Ueno, Sergei I Grivennikov, Francesca Lovat, et al. MicroRNA-135b promotes cancer progression by acting as a downstream effector of oncogenic pathways in colon cancer. *Cancer Cell*, 25(4):469–483, 2014.
- [53] Sabina Halappanavar, Jake Nikota, Dongmei Wu, Andrew Williams, Carole L Yauk, and Martin Stampfli. IL-1 receptor regulates microRNA-135b expression in a negative feedback mechanism during cigarette smoke-induced inflammation. *Journal of Immunology*, 190(7):3679–3686, 2013.
- [54] Edward T Morgan. Regulation of cytochrome p450 by inflammatory mediators: why and how? *Drug Metabolism and Disposition*, 29(3):207–212, 2001.
- [55] Emily Shacter and Sigmund A Weitzman. Chronic inflammation and cancer. *Oncology (Williston Park, NY)*, 16(2):217–26, 2002.
- [56] Alberto Mantovani, Paola Allavena, Antonio Sica, and Frances Balkwill. Cancer-related inflammation. *Nature*, 454(7203):436–444, 2008.
- [57] Francesco Colotta, Paola Allavena, Antonio Sica, Cecilia Garlanda, and Alberto Mantovani. Cancer-related inflammation, the seventh hallmark of cancer: links to genetic instability. *Carcinogenesis*, 30(7):1073–1081, 2009.
- [58] Fran Balkwill and Alberto Mantovani. Inflammation and cancer: back to virchow? *Lancet*, 357(9255):539–545, 2001.
- [59] Gareth Catchpole, Alexander Platzer, Cornelia Weikert, Carsten Kempkensteffen, Manfred Johannsen, Hans Krause, Klaus Jung, Kurt Miller, Lothar Willmitzer, Joachim Selbig, et al. Metabolic profiling reveals key metabolic features of renal cell carcinoma. *Journal of Cellular and Molecular Medicine*, 15(1):109–118, 2011.

- [60] James Ming Phang, Wei Liu, Chad Hancock, and Kyle J Christian. The proline regulatory axis and cancer. *Frontiers in Oncology*, 2, 2012.
- [61] James M Phang, Wei Liu, Chad N Hancock, and Joseph W Fischer. Proline metabolism and cancer: emerging links to glutamine and collagen. *Current Opinion in Clinical Nutrition and Metabolic Care*, 18(1):71, 2015.
- [62] George Adrian Calin, Calin Dan Dumitru, Masayoshi Shimizu, Roberta Bichi, Simona Zupo, Evan Noch, Hansjuerg Aldler, Sashi Rattan, Michael Keating, Kanti Rai, et al. Frequent deletions and down-regulation of micro-rna genes mir15 and mir16 at 13q14 in chronic lymphocytic leukemia. *Proceedings of the National Academy of Sciences*, 99(24):15524–15529, 2002.
- [63] Dan Li, Yulan Zhao, Changxing Liu, Xiaona Chen, Yanting Qi, Yue Jiang, Chao Zou, Xiaolong Zhang, Shunying Liu, Xuejing Wang, et al. Analysis of miR-195 and miR-497 expression, regulation and role in breast cancer. *Clinical Cancer Research*, 17(7):1722–1730, 2011.
- [64] Hongxia Deng, Yanan Guo, Haojun Song, Bingxiu Xiao, Weiliang Sun, Zhong Liu, Xiuchong Yu, Tian Xia, Long Cui, and Junming Guo. MicroRNA-195 and microRNA-378 mediate tumor growth suppression by epigenetical regulation in gastric cancer. *Gene*, 518(2):351–359, 2013.
- [65] Chao Cai, Qing-Biao Chen, Zhao-Dong Han, Yan-Qiong Zhang, Hui-Chan He, Jia-Hong Chen, Yan-Ru Chen, Sheng-Bang Yang, Yong-Ding Wu, Yan-Ru Zeng, et al. miR-195 inhibits tumor progression by targeting RPS6KB1 in human prostate cancer. *Clinical Cancer Research*, 21(21):4922–4934, 2015.
- [66] Jia Guo, Min Wang, and Xiuheng Liu. MicroRNA-195 suppresses tumor cell proliferation and metastasis by directly targeting BCOX1 in prostate carcinoma. *Journal of Experimental & Clinical Cancer Research*, 34(1):1, 2015.
- [67] Chunhui Liu, Han Guan, Yiduo Wang, Ming Chen, Bin Xu, Lei Zhang, Kai Lu, Tao Tao, Xiaowen Zhang, and Yeqing Huang. miR-195 inhibits EMT by targeting FGF2 in prostate cancer cells. *PloS One*, 10(12):e0144073, 2015.
- [68] Désirée Bonci, Valeria Coppola, Maria Musumeci, Antonio Addario, Raffaella Giuffrida, Lorenzo Memeo, Leonardo D’Urso, Alfredo Pagliuca, Mauro Biffoni, Catherine Labbaye, et al. The miR-15a–miR-16-1 cluster controls prostate cancer by targeting multiple oncogenic activities. *Nature Medicine*, 14(11):1271–1277, 2008.
- [69] D Bonci, V Coppola, M Patrizii, A Addario, A Cannistraci, F Francescangeli, R Pecci, G Muto, D Collura, R Bedini, et al. A microRNA code for prostate cancer metastasis. *Oncogene*, 35:1180–1192, 2016.
- [70] A Petrelli, A Perra, K Schernhuber, M Cargnelutti, A Salvi, C Migliore, E Ghiso, A Benetti, S Barlati, GM Ledda-Columbano, et al. Sequential analysis of multistage hepatocarcinogenesis reveals that miR-100 and PLK1 dysregulation is an early event maintained along tumor progression. *Oncogene*, 31(42):4517–4526, 2012.
- [71] Ping Chen, Xia Zhao, and Liang Ma. Downregulation of microRNA-100 correlates with tumor progression and poor prognosis in hepatocellular carcinoma. *Molecular and Cellular Biochemistry*, 383(1-2):49–58, 2013.
- [72] Yiwu Dang, Dianzhong Luo, Minhua Rong, and Gang Chen. Underexpression of miR-34a in hepatocellular carcinoma and its contribution towards enhancement of proliferating inhibitory effects of agents targeting c-MET. *PloS One*, 8(4):e61054, 2013.

- [73] Na Li, Hanjiang Fu, Yi Tie, Zheng Hu, Wei Kong, Yongge Wu, and Xiaofei Zheng. miR-34a inhibits migration and invasion by down-regulation of c-Met expression in human hepatocellular carcinoma cells. *Cancer Letters*, 275(1):44–53, 2009.
- [74] Qiao Ying, Linhui Liang, Weijie Guo, Ruopeng Zha, Qi Tian, Shenglin Huang, Jian Yao, Jie Ding, Meiyao Bao, Chao Ge, et al. Hypoxia-inducible microRNA-210 augments the metastatic potential of tumor cells by targeting vacuole membrane protein 1 in hepatocellular carcinoma. *Hepatology*, 54(6):2064–2075, 2011.
- [75] Wen Xue, Lars Zender, Cornelius Miething, Ross A Dickins, Eva Hernando, Valery Krizhanovsky, Carlos Cordon-Cardo, and Scott W Lowe. Senescence and tumour clearance is triggered by p53 restoration in murine liver carcinomas. *Nature*, 445(7128):656–660, 2007.
- [76] Guido T Bommer, Isabelle Gerin, Ying Feng, Andrew J Kaczorowski, Rork Kuick, Robert E Love, Yali Zhai, Thomas J Giordano, Zhaohui S Qin, Bethany B Moore, et al. p53-mediated activation of miRNA34 candidate tumor-suppressor genes. *Current Biology*, 17(15):1298–1307, 2007.
- [77] Tsung-Cheng Chang, Erik A Wentzel, Oliver A Kent, Kalyani Ramachandran, Michael Mullendore, Kwang Hyuck Lee, Georg Feldmann, Munekazu Yamakuchi, Marcella Ferlito, Charles J Lowenstein, et al. Transactivation of miR-34a by p53 broadly influences gene expression and promotes apoptosis. *Molecular Cell*, 26(5):745–752, 2007.
- [78] Zhaohui Feng, Cen Zhang, Rui Wu, and Wenwei Hu. Tumor suppressor p53 meets microRNAs. *Journal of Molecular Cell Biology*, 3(1):44–50, 2011.
- [79] Don L Gibbons, Wei Lin, Chad J Creighton, Zain H Rizvi, Philip A Gregory, Gregory J Goodall, Nishan Thilaganathan, Liqin Du, Yiqun Zhang, Alexander Pertsemliadis, et al. Contextual extracellular cues promote tumor cell EMT and metastasis by regulating miR-200 family expression. *Genes & Development*, 23(18):2140–2151, 2009.
- [80] Xiuling Zhang, Ping Li, Minhua Rong, Rongquan He, Xinxi Hou, You Xie, and Gang Chen. MicroRNA-141 is a biomarker for progression of squamous cell carcinoma and adenocarcinoma of the lung: Clinical analysis of 125 patients. *The Tohoku Journal of Experimental Medicine*, 235(3):161–169, 2015.
- [81] Zhoufang Mei, Yanchao He, Jingjing Feng, Jindong Shi, Yong Du, Ling Qian, Qihui Huang, and Zhijun Jie. MicroRNA-141 promotes the proliferation of non-small cell lung cancer cells by regulating expression of PHLPP1 and PHLPP2. *FEBS Letters*, 588(17):3055–3061, 2014.
- [82] B Eghbali, JA Kessler, LM Reid, C Roy, and DC Spray. Involvement of gap junctions in tumorigenesis: transfection of tumor cells with connexin 32 cDNA retards growth in vivo. *Proceedings of the National Academy of Sciences*, 88(23):10701–10705, 1991.
- [83] Edward Leithe, Solveig Sirnes, Yasufumi Omori, and Edgar Rivedal. Downregulation of gap junctions in cancer cells. *Critical Reviews in Oncogenesis*, 12(3-4), 2006.
- [84] Vasudha Sehgal, Elena G Seviour, Tyler J Moss, Gordon B Mills, Robert Azencott, and Prahlad T Ram. Robust Selection Algorithm (RSA) for multi-omic biomarker discovery; integration with functional network analysis to identify miRNA regulated pathways in multiple cancers. *PloS One*, 10(10):e0140072, 2015.
- [85] Hiroshi I Suzuki, Hajime Mihira, Tetsuro Watabe, Koichi Sugimoto, and Kohei Miyazono. Widespread inference of weighted microRNA-mediated gene regulation in cancer transcriptome analysis. *Nucleic Acids Research*, 41(5):e62–e62, 2013.

- [86] Thomas Bleazard, Janine A Lamb, and Sam Griffiths-Jones. Bias in microRNA functional enrichment analysis. *Bioinformatics*, 31:1592–1598, 2015.
- [87] Bo Li and Colin N Dewey. Rsem: accurate transcript quantification from rna-seq data with or without a reference genome. *BMC Bioinformatics*, 12(1):323, 2011.

7 Supplementary Information

7.1 Data and Processing

Preprocessing We downloaded mRNA expression data sets (sequenced on an IlluminaHiSeq RNASeqV2 platform, TCGA data level 3) and miRNA expression data sets (sequenced on an IlluminaHiSeq miRNASeq platform, TCGA data level 3) for primary tumor samples (tissue label “01”) and adjacent-normal samples (tissue label “11”) for breast (BRCA), lung (LUSC), liver (LIHC), and prostate (PRAD) cancers from TCGA. We normalized mRNA libraries such that the sum of all transcripts in each library was one, making them comparable between samples. Afterwards, we filtered out genes which had very low median expression across all samples ($\leq 10^{-9}$ in the “scaled_estimate” column), since several genes had no discernible expression across most samples in the set. The remaining mRNA data were then multiplied by 10^6 to obtain transcripts per million (TPM) as described in [1] and then \log_2 transformed, including the addition of a small offset (10^{-10}) for the \log_2 transformation.

miRNA expression data were downloaded from the same TCGA samples and similarly preprocessed, in which miRNA libraries were normalized such that the sum of all transcripts in each library was one. Afterwards, miRNAs with very low median expression across all samples (≤ 0.001 in the “reads_per_million_miRNA_mapped” column) were filtered out.

Data In breast cancer, 1203 samples (1092 tumor, 111 adjacent-normal) were used to compute the PAS, of which 758 (671 tumor, 87 adjacent-normal) samples were used for class-conditional correlations with 444 miRNAs. In prostate cancer, PAScomputation used 538 samples (486 tumor, 52 adjacent-normal), of which 534 (482 tumor, 52 adjacent-normal) samples were used for class-conditional correlations with 416 miRNAs. Liver cancer PAScomputation used 401 samples (351 tumor, 50 adjacent-normal), of which 397 samples (347 tumor, 50 adjacent-normal) were used for correlations with 397 miRNAs. Finally, lung cancer used 553 samples (502 tumor, 51 adjacent-normal) for PAS, of which 380 samples (342 tumor, 38 adjacent-normal) were used for correlations with 380 miRNAs.

Isomap parameter choice Isomap applies MDS on a distance matrix that approximates geodesic distances, constructed by a k -nearest neighbors search and computing shortest paths. It is a well known result that classical MDS (using euclidean distance) and PCA produce identical spectra, with extra zero eigenvalues accounting for the difference in input dimensions. This is because the rank of the data is the same. Mathematically, this is demonstrated as follows: if X is an input matrix, spanning s samples by g genes (mean centered), the spectra of $X^T X$ and $X X^T$ will be identical, with extra $s - g$ zero eigenvalues. Therefore, in the high- k limit, Isomap and PCA will produce identical spectra because the distance matrix is euclidean and no geodesic distances will be imputed.

7.2 Systems Effects

Because our method relies on statistical associations, it does not necessarily select miRNAs and pathways having known biological relationships. We therefore tested all miRNA-pathway pairs to determine whether altered associations were more likely to be enriched with predicted miRNA targets. Each miRNA’s predicted mRNA targets were taken from TargetScan and significance was assessed using a hypergeometric test. Scatterplots of enrichment vs. altered association are shown in Figure 8. Target enrichment did not correlate well with $\Delta\rho$ significance in each cancer type (all $\rho < 0.1$).

It should be noted that other potential explanatory mechanisms did not explain flagged miRNA-pathway relationships. We found poor association between miRNA differential expression (using a Student’s t -test) and the number of flagged pathways with each miRNA in each organ type, shown in Figure 9. Additionally,

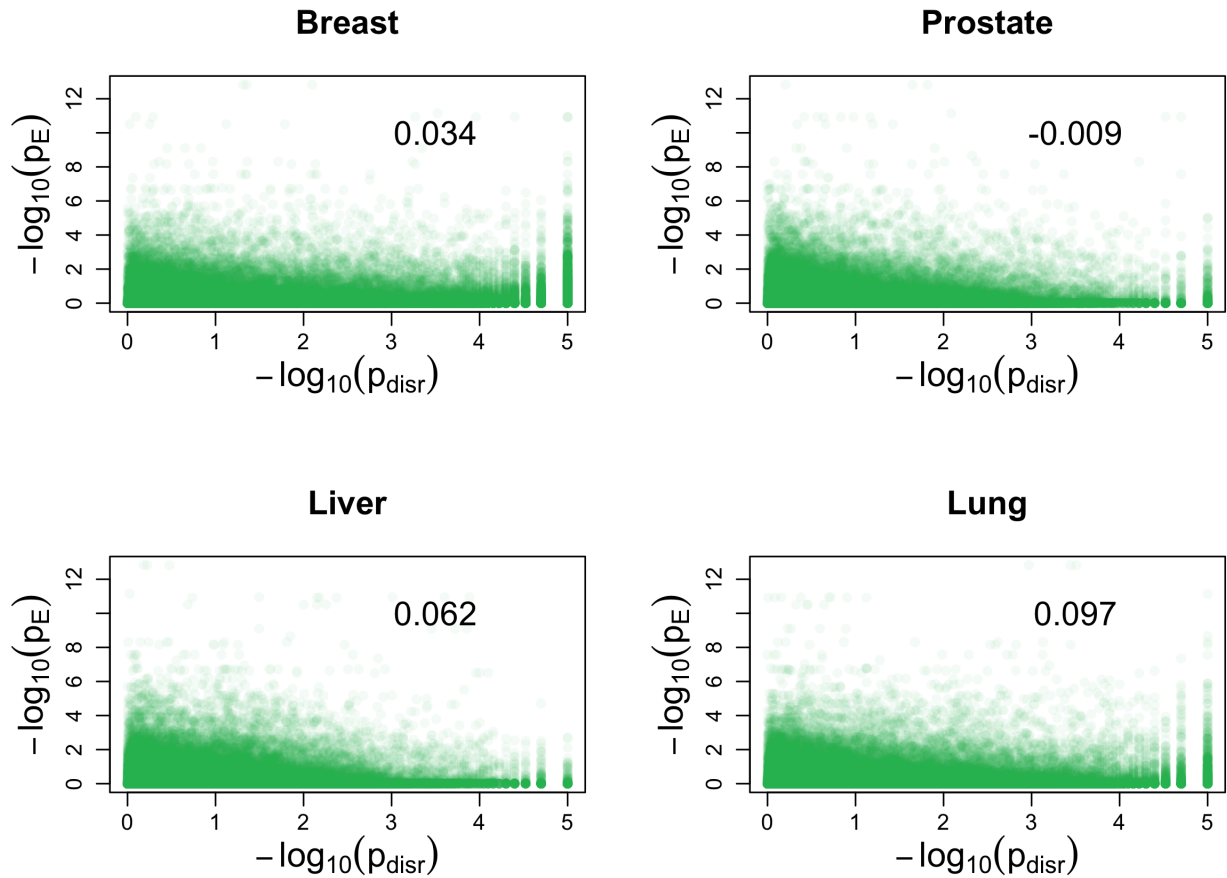


Figure 8: Scatterplots of enrichment significance ($-\log_{10} p_E$) vs. $\Delta\rho$ significance ($-\log_{10} p_{disr}$) for all miRNA \times pathway pairs within each cancer type. Rank correlations are displayed within each figure.

we investigated whether larger pathways are more likely to be flagged since they invariably contain more miRNA targets. We also found poor association between pathway size and significance, shown in Figure 10. These results suggest that differential regulations are likely driven by systems effects, rather than by specific individual interactions or scale effects.

7.3 Cross-cancer comparison

We illustrate the comparison of all miRNA–pathway pairs across different organs using a scatterplot matrix of their $\Delta\rho$ significance, shown in Figure 11. Cancer types exhibit poor concordance with one another, since the Spearman’s rank correlation of their miRNA–pathway pairs’ p -values are fairly low (shown in the upper right panels). This discordance may be visualized by the lower heat map panels of p -value density. High concordance would be evidenced by high density (darker colors) along the diagonal, which is not observed. Instead, high density is located in regions with low significance in at least one or both cancers being compared. Thus, each cancer type appears to contain a unique profile of miRNA–pathway relationships which are significantly changed in tumor tissue. This may be attributable to the fact that the PAS is computed conditional on cancer type, which could distort cross-cancer comparisons.

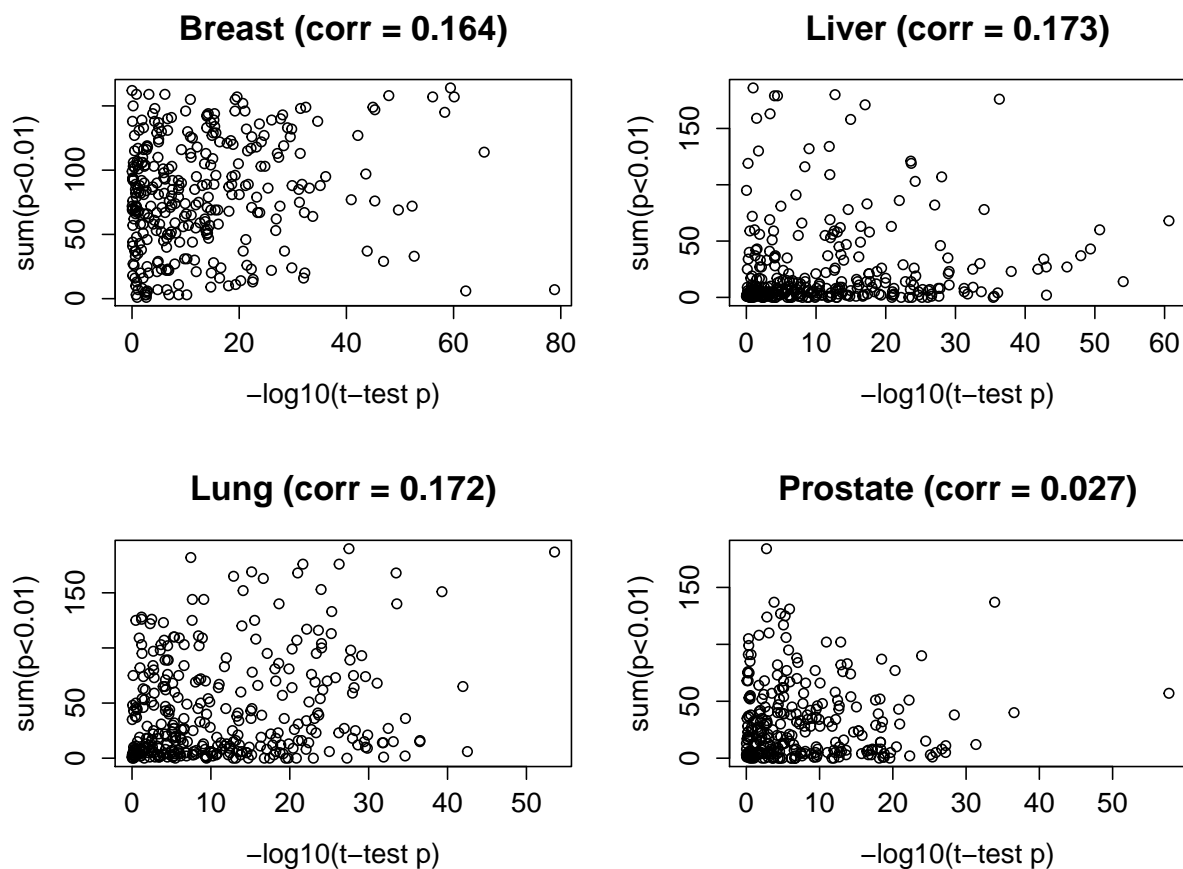


Figure 9: Marginal miRNA differential expression, as calculated by Student’s t -test between tumor and adjacent-normal tissue, does not determine the number of pathways differentially regulated by a miRNA ($p < 0.01$).

It is notable that within each cancer type, there are more pairs with significant $\Delta\rho$ than expected by chance alone. The diagonal panels in Figure 11 illustrate the within-cancer $-\log_{10} p$ distributions, in which breast cancer has by far the largest proportion of significant pairs out of all pairs investigated, followed by lung, prostate, and finally liver cancer. In general, a multitude of miRNA regulatory effects at the pathway level appear to be disrupted, in agreement with the literature implicating broad miRNA dysregulation in tumors.

References

- [1] Ambros, L. and Dewey, C.N. (2011) RSEM: accurate transcript quantification from RNA-Seq data with or without a reference genome. *BMC Bioinformatics*, **12**, 323.

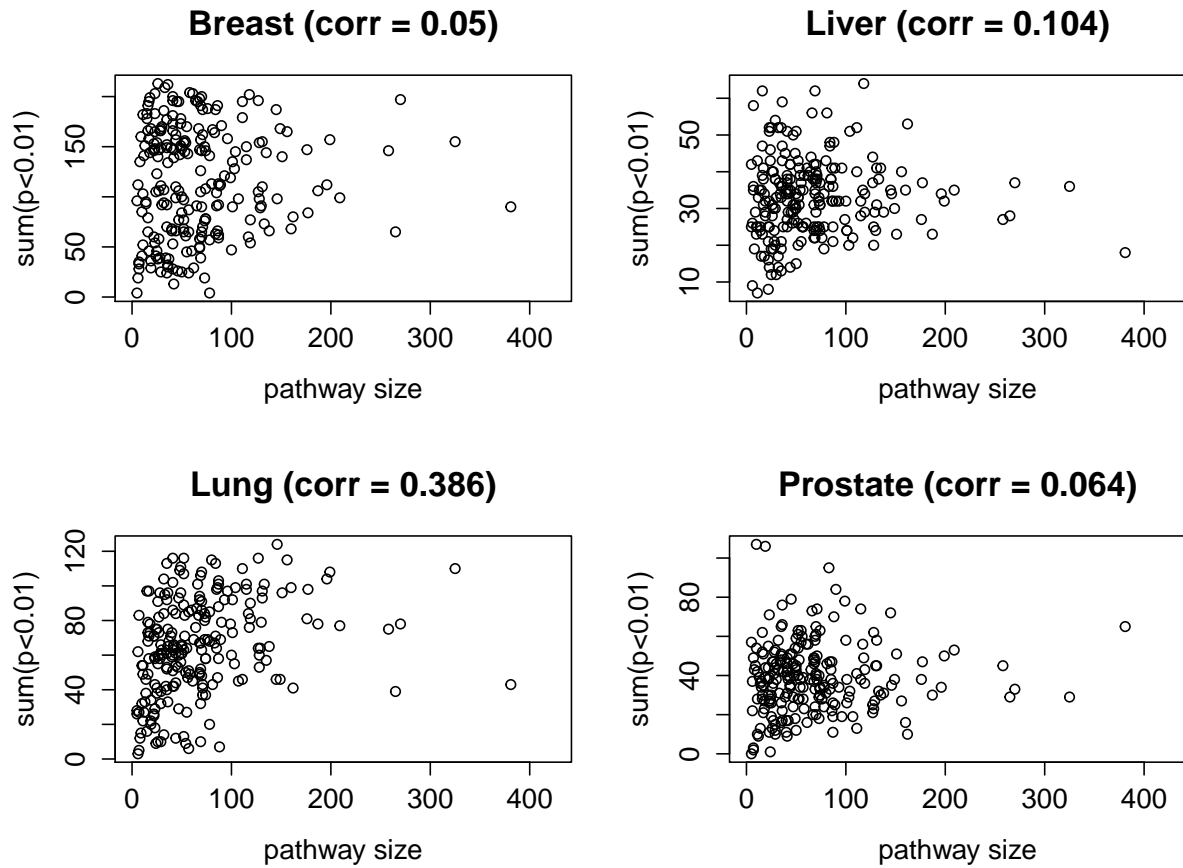


Figure 10: Pathway size does not generally influence pathway significance. The size of the pathway does not correlate appreciably with the number of miRNAs differentially regulating ($p < 0.01$) that pathway. Lung cancer does appear to have a size-dependence unlike the other cancers.

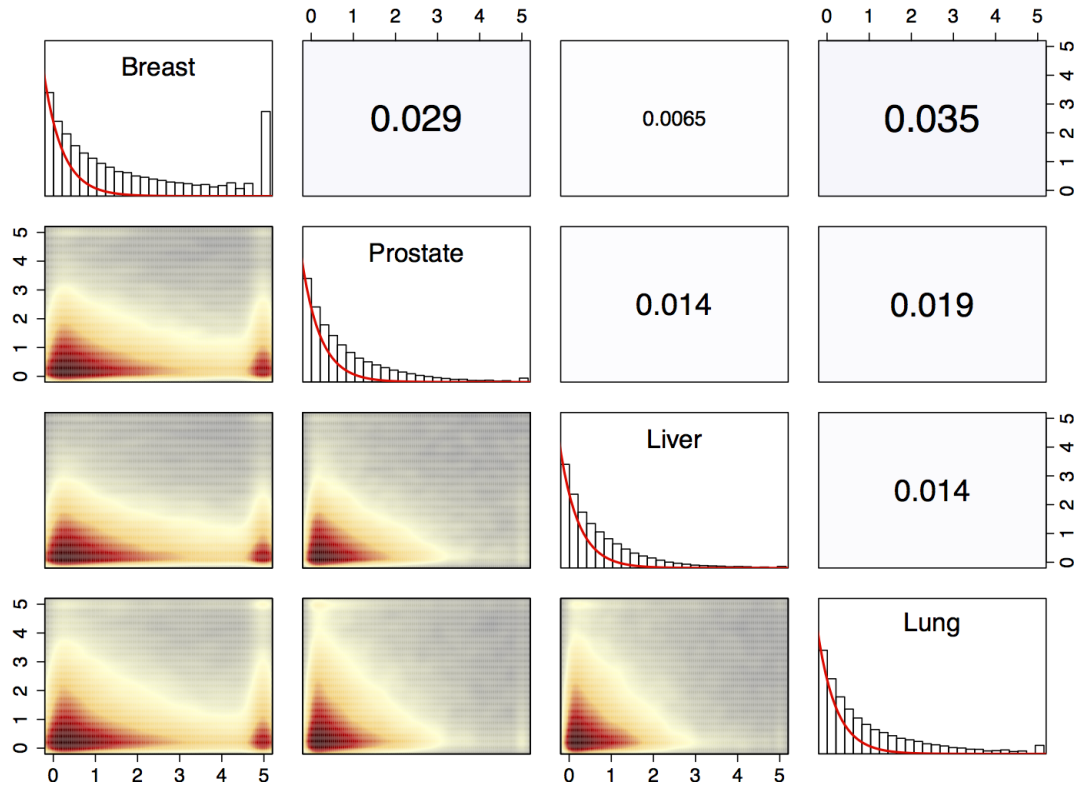


Figure 11: Scatterplot matrix showing the significance of $\Delta\rho$ for all miRNA–pathway pairs across cancer types. Lower panels display the scatterplot density heat map for $-\log_{10} p$ between cancer types, in which darker colors denote higher density. Diagonal panels display $-\log_{10} p$ histograms within each cancer type, overlaid with $-\log_{10} p$ null distribution drawn by the red curve. Upper panels display the Spearman correlation coefficient of p -values between cancer types across all pairs.